# Carboxy SNARF-4F as a Fluorescent pH Probe for Ensemble and Fluorescence Correlation Spectroscopies

**ARTICLE** *in* THE JOURNAL OF PHYSICAL CHEMISTRY B · JULY 2005

Impact Factor: 3.3 · DOI: 10.1021/jp0510138 · Source: PubMed



**2 AUTHORS:**

Nathalie Marcotte
Ecole Nationale Supérieure de Chimie de Mo…
**28** PUBLICATIONS **600** CITATIONS
SEE PROFILE

Albert M Brouwer
University of Amsterdam
**142** PUBLICATIONS **3,421** CITATIONS
SEE PROFILE

# Carboxy SNARF-4F as a Fluorescent pH Probe for Ensemble and Fluorescence Correlation Spectroscopies

**Nathalie Marcotte[†] and Albert M. Brouwer***

*Van't Hoff Institute for Molecular Sciences, University of Amsterdam, Nieuwe Achtergracht 129, 1018 WS Amsterdam, The Netherlands*

*Received: February 28, 2005; In Final Form: April 9, 2005*

The optical spectroscopic properties of 1,4(and 5)-benzenedicarboxylic acid, 2-[10-(dimethylamino)-4-fluoro-3-oxo-3H-benzo[*c*]xanthen-7-yl] (carboxy SNARF-4F), a commercial promising fluorescent pH probe, are investigated in buffered aqueous solutions in the 5.6−8.2 pH range by steady-state and time-resolved spectroscopy. A multiexponential global analysis of the picosecond time-resolved data is performed. The nonprotonated A* species decays monoexponentially (0.73 ns), while the protonated species AH* decays following a biexponential law with time constants of 0.40 and 1.87 ns. A kinetic scheme is proposed to explain the observations, which involves AH* in equilibrium with a species denoted Y*. The nature of Y* is discussed in terms of a possible structural change in the molecule producing the lactone form, although the formation of a hydrogen-bonded complex to the solvent cannot be ruled out. Finally, the ability of the dye to probe pH at the single-molecule level is explored using fluorescence correlation spectroscopy.

## Introduction

The concentration of $H^+$ ions plays an important role in biological media, more particularly, in cellular processes such as cell growth, apoptosis, muscle contraction, ion transport, endocytosis, or tumor cells. Apart from cellular biology, other fields of interest of pH sensing especially include agricultural chemistry, food industry, environmental chemistry, the pharmaceutics industry, and human health.

Among the noninvasive methods that exist to monitor pH, the ones based on fluorescence techniques have been the most extensively employed in recent years due to the great sensitivity and the high spatial resolution they provide.[1] Moreover, fluorescence spectroscopy allows remote sensing with fiber optics[2−4] and is well suitable for single-molecule detection.[5−8]

The sensing action of a fluorescent pH probe is usually signaled through a fluorescence change of the solution upon direct binding of the dye by a proton. Depending on the photophysical properties of the neutral and charged forms, two different classes of indicators can be distinguished. The first one includes most of the compounds commonly used, among which are derivatives of fluorescein, anthracene, or pyrene. In this class, only one of the two forms, acid or base, exhibits a significant fluorescence, so that the pH-related variations of the fluorescence intensity simply follow the absorption changes of the emitting species, that is, its concentration. For the indicators belonging to the second class, the acid and base forms possess specific characteristic fluorescence and/or absorption bands. They thus respond to pH changes by shifts in emission or excitation spectra. Such shifts are of particular interest, since they allow ratiometric measurements, whereby the ratio of the fluorescence at two different wavelengths is independent of the overall dye concentration, photobleaching, and changes of instrumental conditions such as optical path length, excitation intensity, or detector sensitivity. While the latter category is very promising, only limited practical examples of ratio-able emission systems have found an application prior to the development in the early 1990s of benzo[*c*]xanthene dyes such as carboxy seminaphthofluoresceins (SNAFLs) and carboxy seminaphthorhodafluors (carboxy SNARFs).[9] Among these indicators, carboxy SNARF-1 has found numerous applications in cellular biology,[10−15] owing to the suitability of its p$K_a$ (∼7.5) for measurements under physiological conditions. Fluorination of carboxy seminaphthorhodafluors[16] was further performed to lower the p$K_a$ value of carboxy SNARF-1. On the basis of meagerly detailed steady-state fluorescence measurements,[16] one of the resulting compounds (carboxy SNARF-4F, Scheme 1) was reported to possess a p$K_a$ of ∼6.4, attractive to trace the pH evolution in acidic cellular compartments.

Fluorescence-lifetime-based sensing offers the same advantages as fluorescence wavelength ratiometric measurements.[17] However, with the fluorescence lifetime being an intrinsic property of the fluorophore, special design of the molecule is required to implement a pH sensor. This can be achieved for example using the principle of quenching via photoinduced electron transfer.[18−20] Alternatively, the use of dual-emissive probes permits circumvention of this problem. By taking benefit of the overlap of the acid and base emission bands, a titration curve can be constructed from the ratio of both amplitudes, provided the decay times are different enough.[21,22]

The emergence of single-molecule spectroscopy tools such as fluorescence correlation spectroscopy (FCS) in recent years has opened new perspectives for pH sensing applications. Nowadays, numerous studies commonly use the intrinsic properties of autofluorescent biomolecules, like green fluorescence proteins (GFPs), for pH sensing purposes.[23−25]

Whereas carboxy SNARF-4F has been claimed to be a very promising fluorescent sensitive pH probe in the 6−7.5 pH range,[16] no investigation making use of the indicator has been reported to date, to the best of our knowledge.[16] A full

* To whom correspondence should be addressed. Phone: (+31) 205255491. Fax: (+31) 205255670. E-mail: A.M.Brouwer@uva.nl.
[†] Present address: Hétérochimie Moléculaire et Macromoléculaire (CNRS UMR 5076), Ecole Nationale Supérieure de Chimie de Montpellier, France.

10.1021/jp0510138 CCC: $30.25 
Published on Web 05/20/2005

**SCHEME 1: Ground-State Equilibrium between the Acid (AH) and Base (A) Forms of Carboxy SNARF-4F and Chemical Structure of the Neutral Lactone Form (L)**

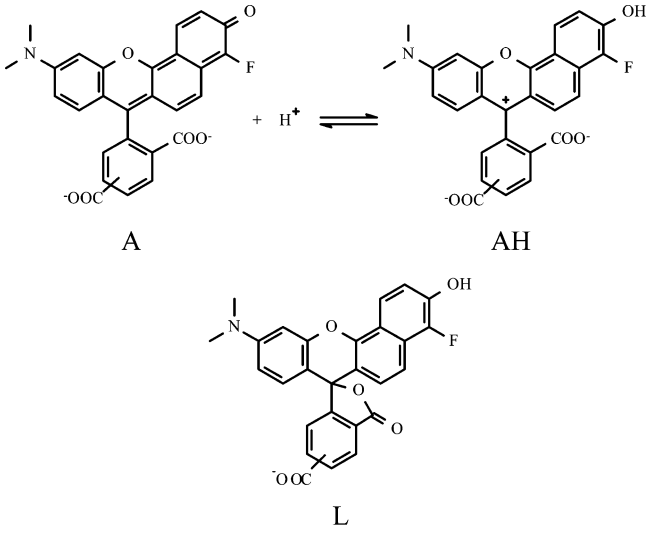


characterization of its optical spectroscopic properties would undoubtedly support the development of its utilization for analytical or biological applications. In the present article, we report on a detailed study of the spectroscopic and photophysical behavior of carboxy SNARF-4F in buffered solutions using steady-state and time-resolved spectroscopy. We also address its potential application as a single-molecule pH probe by means of FCS analysis.

## Experimental Section

**Materials.** Carboxy SNARF-4F was purchased from Molecular Probes, Inc. It was purified by thin-layer chromatography on silica gel with methanol/ethyl acetate (60:40) as the eluant. Buffers appropriate for the desired pH were prepared at a concentration of 10 mM and a constant ionic strength of 50 mM (adjusted with KCl) from anhydrous monobasic/dibasic potassium phosphate, potassium acetate/glacial acetic acid, and 2-[*N*-morpholino]ethanesulfonic acid potassium salt/2-[*N*-morpholino]ethanesulfonic acid hydrate, all purchased from Sigma and used without further purification. All the solutions were prepared in pure water of 16.6 MΩ cm typical resistivity produced on a Nanopure purification system (Barnstead).

**Ensemble Measurements.** In all the experiments performed at the ensemble level, the sample concentration was $1.3 \times 10^{-6}$ M.

*Steady-State Measurements*. UV−vis absorption spectra were recorded on a Cary 3 spectrophotometer (Varian). Cuvettes of 5 cm optical path length were used, allowing the same concentrations for absorbance and fluorescence measurements to be monitored with a good accuracy. Steady-state fluorescence spectra were measured on a Spex Fluorolog 3 spectrofluorometer (Jobin-Yvon) equipped with a 1 cm light path cell holder thermostated at 20 °C. All fluorescence spectra were corrected for the wavelength dependence of the response of the detection system.

*Time-Resolved Fluorescence*. Time-resolved fluorescence was acquired using the time-correlated single-photon counting (TCSPC) technique by two distinct pieces of equipment: an in-house assembled TCSPC setup and a commercial confocal microscope, MicroTime 200, from PicoQuant GmbH. The TCSPC setup has been described elsewhere.[26] Briefly, laser excitation (323 nm) was achieved by frequency doubling the

**SCHEME 2: Confocal Microscope Setup for Dual Color Detection**[a]

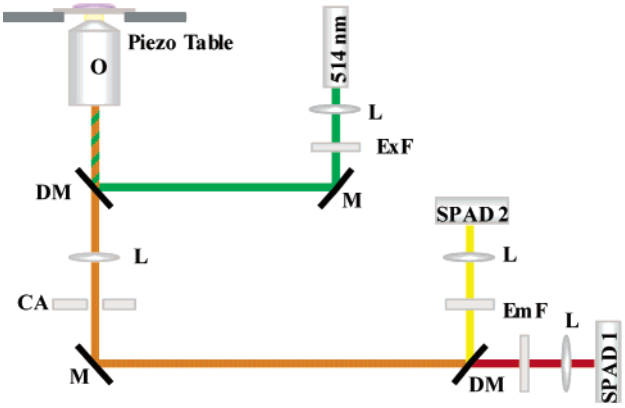


[a] CA, confocal aperture; DM, dichroic mirror; ExF, excitation filter (D510/20x); EmF, emission filter (D660/50m on SPAD 1 and D580/25m on SPAD 2); L, lens; M, mirror; O, oil-immersion objective (100×, NA 1.3)

output of a cavity dumped DCM dye laser (Coherent model 700) pumped by a mode-locked $Ar^+$ laser (Coherent 486 AS Mode Locker, Coherent Innova 200 laser). To exclude polarization effects, fluorescence was collected under the magic angle (54.7°). A microchannel plate (Hamamatsu R3809) was used as the detector. The overall instrumental response function (IRF), measured from Raman scattering of doubly deionized water, was ~20 ps (fwhm). Decay curves were collected at 570, 625, and 670 nm in 4000 channels (1.25 ps/channel) with about 8000 detected counts at the maximum of the fluorescence signal. Each decay trace was recorded three times from independent solutions after an IRF was measured.

Scheme 2 shows the confocal setup used in our experiments. The 514 nm line of the $Ar^+$ laser previously described was collimated into a polarization-maintaining single-mode fiber. The laser light passed an excitation filter (D510/20x, Omega Optical) and was directed to a Berek polarization compensator (New Focus 5540) in order to change the beam polarization from linear to circular. Light was directed into a high-aperture oil-immersion objective (100×, NA 1.3, Olympus) of an inverted microscope (Olympus IX71) by a dichroic beam splitter (540DCLP, Omega Optical). The fluorescence signal was collected by the same objective and transmitted through the dichroic mirror. A tube lens focused the light onto a 150 $\mu$m pinhole for confocal imaging. After the pinhole, the light was split by a dichroic mirror (610DCLP, Omega Optical), which permits two-channel detection and was refocused by two lenses onto the active areas of two single-photon avalanche diodes (SPCM CD2801 from Perkin-Elmer, denoted here as SPAD 1 and SPAD 2). Two emission band-pass filters were placed in front of the SPADs (D660/50m on SPAD 1 and D580/25m on SPAD 2, Omega Optical) to further discriminate fluorescence from scattered light and to selectively collect the long-wavelength part of the fluorescence spectrum (largely due to the deprotonated SNARF-4F) on SPAD 1 and the shorter wavelength part (largely due to the protonated form) on SPAD 2. Data acquisition was performed with a PC equipped with a TimeHarp 200 TCSCP board (PicoQuant), which permits one to collect the signal in up to 4096 channels with a time increment smaller than 40 ps and to continuously record photon arrival times with 100 ns time resolution. The timing electronics was synchronized with the pulsed excitation (76 MHz repetition rate) using a TDA 200 photodiode (from PicoQuant). The instrument

response function of the entire system was measured to be 460 ps (fwhm) on SPAD 1 and 540 ps (fwhm) on SPAD 2.

**Fluorescence Correlation Measurements.** The solutions for fluorescence correlation spectroscopy (FCS) experiments were prepared by diluting a stock solution of the dye ($1.75 \times 10^{-5}$ M stored at −20 °C until use) with the appropriate amount of buffer down to the required concentration of $8.75 \times 10^{-9}$ M. A drop of the solution was placed in a cover slip well formed with silicone isolator spacer and sealed by another cover slide. Measurements were performed using the confocal setup just described above. Excitation and detection occurred at a distance of ~8 $\mu$m above the surface of the cover slip. Each sample was measured five times over an acquisition period of 300 s. The number of experiments, their duration, and the high count rates facilitated by the 150 $\mu$m pinhole size were necessary to obtain a good signal-to-noise ratio. Only samples having a signal-to-background ratio >10 were analyzed. The time-tagged time-resolved (TTTR) data acquisition mode used allows the processing of FCS curves, multichannel scaling (MCS) traces, and TCSPC histograms from a single measurement. All these fluorescence analyses were performed using MicroTime 200 software, version 3.1.

The normalized autocorrelation function ($G(\tau)$) is defined as

$$G(\tau) = \frac{\langle \delta I(t)\, \delta I(t+\tau)\rangle}{\langle I(t)\rangle^2} \quad (1)$$

where $\delta I(t) = I(t) - \langle I(t)\rangle$, $I(t)$ denotes the fluorescence intensity, $\langle I(t)\rangle$ its mean, and $\tau$ the delay time. The autocorrelation curves obtained from the same sample, very similar for the five runs, were averaged to improve the signal-to-noise ratio before being analyzed with the following equation:

$$G(\tau) = \frac{1}{N}\left(\frac{1}{1+4D\tau/\omega^2}\right)(1 - T + T\exp(-\tau/\tau_T)) \quad (2)$$

in which the first term describes a freely diffusing fluorescent species in a 2D-Gaussian observation volume, $N$ denotes the average number of molecules, $D$ the translational diffusion coefficient, and $\omega$ the $1/e^2$ radius of the Gaussian profile of the laser beam focus in the radial direction. The second term stands for the fluorescence fluctuations arising from molecules entering and leaving a dark state, as for instance a triplet state; $T$ denotes the mean fraction of fluorophores in that state, and $\tau_T$ is the relaxation time. It is worth noting that good fits were obtained using an only 2D-Gaussian focal volume description and that underfilling the back-aperture of the objective did not allow a better description of the volume using a 3D model.[27]

The stability of the optical setup, in particular the size of the measurement volume, was routinely checked by FCS calibration using rhodamine 6G (R6G). In that case, fitting of the autocorrelation curves resulted in good results without the need of the second term of eq 2. The typical beam waist radius of the focused laser beam was found to be ~230 nm at $1/e^2$ relative intensity, assuming a diffusion coefficient of $D = 2.8 \times 10^{-6}$ cm$^2$/s for R6G in water.[28]

**Global Data Analysis.** Global data analyses were performed on steady-state and time-resolved data using two distinct approaches: a global fitting procedure and a modeling process.

*Fitting the Data*. The time-resolved fluorescence decay traces recorded with the TCSPC setup were analyzed using a global analysis program (TRFA) from Katholieke Universiteit Leuven,[29,30] which is based on a least-squares iterative convolution of the instrument response to a sum of the exponential decays, according to

$$I(\lambda,t) = \sum_i \alpha_i(\lambda)\exp(-t/\tau_i) \quad (3)$$

where $\tau_i$ is the decay time of the $i$th component and $\alpha_i(\lambda)$ its preexponential factor at the emission wavelength ($\lambda$). This model assuming that $\tau_i$ is independent of $\lambda$ allows the decay curves measured at different emission wavelengths to be analyzed simultaneously.

The goodness of the fits was judged by the reduced $\chi_r^2$ values as well as by visual inspection of the distribution of the weighted residuals and the autocorrelation function of the residuals for each fitted data set. The entire data set consists of a data surface of decays measured at three emission wavelengths for seven different pHs, except at 570 nm where the low count rate of solutions at pH 7.4 and 8.2 did not allow decay traces to be recorded. Each fluorescence trace was first individually analyzed using the minimum number of exponentials required to obtain good fits (usually one to three exponentials). Then, decays recorded for the solutions of different pH were analyzed globally at a single wavelength by linking the decay times. Two exponentials were necessary at 570 nm, and two to three, at 625 and 670 nm. Finally, all the decay curves (19 traces) were analyzed simultaneously at the three wavelengths with linked decay times.

*Modeling and Fitting of the Data*. Modeling and fitting of the data were achieved using the simulation-adjustment software *Sa*, version 3.1, developed by D. Lavabre (Université Paul Sabatier, Toulouse, France). The user interface programming part describing the model has to be adapted to each specific problem. The model describes the evolution of variables as a function of the independent variable (time, concentration, etc.) in terms of a differential (or algebraic) system of equations. The differential equation system is numerically integrated using a semiimplicit Runge−Kutta integrator,[31] and the algebraic equation system is numerically solved by an iterative method. The calculated overall error (sum of the squares of the differences between the experimental and calculated values, otherwise specified) is minimized by a nonlinear least-squares minimization procedure, according to the Powell algorithm.

Absorption data modeling and fitting was carried out to investigate the ground-state equilibrium between A and AH species. The concentrations at equilibrium were calculated solving the equation system 4 and 5:

$$K_1[\mathrm{A}][\mathrm{H}] - [\mathrm{AH}] = 0 \quad (4)$$

$$[\mathrm{AH}] = [\mathrm{A}]_0 - [\mathrm{A}] \quad (5)$$

where [H] is the $H^+$ concentration of the buffered solution, $[A]_0$ the total concentration of A, and $K_1$ ($=k_1/k_{-1}$) the equilibrium constant. The concentrations were connected to absorption data using the Beer−Lambert law:

$$A_T(\lambda) = l(\epsilon_{A(\lambda)}[\mathrm{A}] + \epsilon_{AH(\lambda)}[\mathrm{AH}]) \quad (6)$$

in which $\epsilon_{i(\lambda)}$ refers to the molar absorption coefficient of species $i$ at the observation wavelength ($\lambda$), $l$ is the optical path length, and $A_T(\lambda)$ is the total absorbance of the solution at $\lambda$. Fitting was performed simultaneously at two absorption wavelengths by refining the absorption coefficients and $K_1$.

Steady-state fluorescence data were analyzed assuming no interconversion between species in the excited state. In that case, the concentration of the excited species is simply proportional to their concentration in the ground state, that is, directly related to the ground-state equilibrium. The fluorescence intensity ($I_f$)

**SCHEME 3: Kinetic Model of the Deactivation Pathways of the Acid (AH) and Base (A) Forms of Carboxy SNARF-4F**

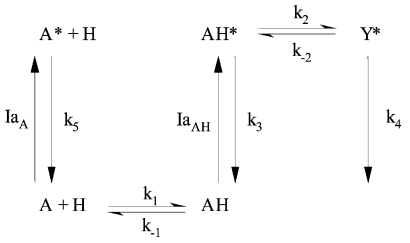


observed at wavelength $\lambda$ is thus defined as

$$I_f = \alpha I_0 l \frac{(1 - 10^{-A_T(\lambda_{exc})})}{A_T(\lambda_{exc})}(q_A[A]\epsilon_{A(\lambda_{exc})} + q_{AH}[AH]\epsilon_{AH(\lambda_{exc})}) \quad (7)$$

where $\alpha$ is the collection efficiency, $I_0$ the photon flux at the excitation wavelength, and $q_i$ the spontaneous emission coefficient of species $i$ at $\lambda$. $A_T$, $\epsilon$, and $l$ have the same meaning as defined above, and $\lambda_{exc}$ refers to the excitation wavelength. Fitting was performed simultaneously at 22 fluorescence emission wavelengths by refining $\alpha I_0$, $q_i$, and $K_1$. Values of $\epsilon_{A(\lambda_{exc})}$ and $\epsilon_{AH(\lambda_{exc})}$ were known independently from the absorption data treatment.

Picosecond time-resolved fluorescence data were analyzed according to the overall kinetic model depicted by Scheme 3. The time-dependent evolution of the excited-state populations is determined by the following differential equations:

$$d[AH^*]/dt = I_0(t)(1 - 10^{-A_T(\lambda_{exc})})\frac{A_{AH}(\lambda_{exc})}{A_T(\lambda_{exc})} + k_{-2}[Y] - (k_2 + k_3)[AH^*] \quad (8)$$

$$d[A^*]/dt = I_0(t)(1 - 10^{-A_T(\lambda_{exc})})\frac{A_A(\lambda_{exc})}{A_T(\lambda_{exc})} - k_5[A^*] \quad (9)$$

$$d[Y^*]/dt = k_2[AH^*] - (k_{-2} + k_4)[Y^*] \quad (10)$$

The first term in eqs 8 and 9 describes the pumping process of the ground-state species AH and A, respectively. $A_T$ is the total absorbance. $I_0(t)$ takes into account the shape of the experimental excitation pulse and the number of incident photons in the excited volume needed to observe a signal of ~8000 counts/s at the maximum of the fluorescence. The number of incident photons per excitation pulse is assumed to only marginally disturb the concentration of ground-state species, so that absorbance can be considered as time-independent. The differential equation system 8−10 was numerically integrated. For each decay trace, a time shift was introduced as an adjustable parameter in the pumping process to account for small time shifts between recorded experimental pulse and sample decay. The concentrations were then used to calculate the fluorescence intensity ($I_f(t)$) observed at wavelength $\lambda$ as follows:

$$I_f(t) = q_{A^*}[A^*] + q_{AH^*}[AH^*] + q_{Y^*}[Y^*] + I_b \quad (11)$$

where $q_i$ is the spontaneous emission coefficient of species $i$ accounting for the fluorescence observed at $\lambda$. $I_b$ is an offset parameter fixed to the background observed in channels preceding the pumping (usually lower than 10 cps). A minimization procedure was simultaneously performed at three wavelengths on seven different pH solutions using a weighted error function defined as $\sum[(\text{calcd} - \text{exptl})^2/\sqrt{\text{exptl}}]$, in which calcd stands for calculated values and exptl stands for experimental data.

## Results and Discussion

The fluorinated carboxy seminaphthorhodafluor 1,4(and 5)-benzenedicarboxylic acid, 2-[10-(dimethylamino)-4-fluoro-3-oxo-3H-benzo[*c*]xanthen-7-yl] (carboxy SNARF-4F) is depicted in Scheme 1 in its protonated (AH) and deprotonated (A) forms. Like fluorescein and rhodamine derivatives bearing a nonesterified carboxylphenyl group,[32,33] carboxy SNARF-4F may also exist in a lactone form. It is commonly accepted that the existence of the various molecular forms depends on the solvent polarity and proticity. Nonpolar and aprotic solvents favor the lactone species, whereas the acid and base forms are strongly stabilized in polar protic media due to hydrogen-bond formation between the carboxyl group and the hydrogen-bond-donating solvent.[34] We investigated the prototropic equilibrium of carboxy SNARF-4F in buffered aqueous solutions, for which the only expected predominating species are the base and acid forms; we focused our studies in the main 5.6−8.2 pH range, where protonation of the carboxyl groups is unlikely. All the measurements were performed at a low buffer concentration (10 mM, constant ionic strength of 50 mM), which reduces the probability of excited-state proton exchange reactions.[35,36] We first present the carboxy SNARF-4F behavior in bulk solution before reporting on its suitability for single-molecule measurements.

**Absorption Spectroscopy.** The spectroscopic behavior of carboxy SNARF-4F resembles that observed for the parent compound carboxy SNARF-1.[9] The UV−vis absorption spectrum of carboxy SNARF-4F ($1.3 \times 10^{-6}$ M) recorded in basic media (pH 9) exhibited an intense band at 582 nm, which further decreased and shifted to the blue upon acidification of the solution. At low pH values (4.6), a new band appeared at shorter wavelengths, peaking at 520 nm. The absorption changes also revealed the presence of isosbestic points at 544, 446, and 404 nm, which reflect a ground-state acid−base equilibrium involving two species. The pH-dependent absorption changes were analyzed according to the following model:

$$A + H \underset{k_{-1}}{\overset{k_1}{\rightleftharpoons}} AH$$

where A and AH stand for the deprotonated and protonated species, respectively. H represents the proton, and $K_1$ ($=k_1/k_{-1}$) is the association constant. Fitting was performed simultaneously at the two absorption wavelengths (510 and 590 nm) where absorbance changes were the largest. Results of the fits are illustrated in Figure 1 (inset). The calculated value for the association constant was $K_1 = (3.06 \pm 0.10) \times 10^6\ M^{-1}$ which corresponds to a p$K_a$ of 6.49, in agreement with the reported value of 6.4.[16] Data processing was then performed at 22 wavelengths by only refining the molar extinction coefficients ($K_1$ fixed to its previously determined value), which allows the UV−vis absorption spectra of both species to be reconstructed (Figure 1).

The blue-shifted absorption spectrum of AH compared to that of A can be interpreted in view of the intramolecular charge transfer character of the bands, resulting from the electron density displacement from the electron-donating dimethylamino group toward the electron-withdrawing carbonyl group upon light irradiation. Protonation of the carbonyl induces a reduction in the $\pi$-conjugated electron system of the xanthene part, which

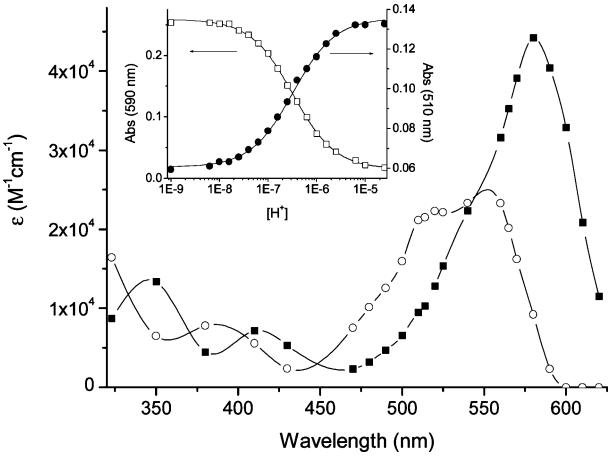


**Figure 1.** Absorption spectra of A (■) and AH (○) species reconstructed from the absorption data processing (the solid lines are smooth curves joining the calculated points to help in visualizing the spectra). Inset: absorbance of carboxy SNARF-4F ($1.3 \times 10^{-6}$ M) versus $H^+$ concentration at 510 nm (●) and 590 nm (□). The symbols represent experimental data, and the solid lines were calculated by fitting the data.

results in an increase in the energy of the electronic transition. Concerning the lactone forms, it is known that their chromophore does not absorb in the visible part of the spectra due to disruption in the $\pi$-conjugation of the xanthene moiety caused by cyclization.[37] Although very often considered as unlikely in water, the absence of the lactone form in our measurements cannot be completely ruled out. As a matter of fact, Hinckley et al.[38] established the existence for rhodamine B lactone in water and quantified its presence at 18.5%.

**Steady-State Fluorescence Spectroscopy.** Fluorescence emission spectra were recorded following excitation at 410 and 514 nm (Figure 2). Solutions predominantly containing the protolytic A form (pH > 7.2) exhibit a long-wavelength band with a maximum situated at 661 nm, which drops and slightly shifts to the blue upon acidification of the solution. The changes are accompanied by the appearance of a new band peaking at 592 nm, which can be assigned to the fluorescence of the protonated species. Upon excitation at 410 nm (Figure 2a), a pseudoisoemissive point is seen at 615 nm. The fluorescence intensity at the maximum of the short-wavelength band of the pH 4.6 solution represents 35% of that observed at 661 nm for pH 8.2. When the excitation wavelength is set at 514 nm (Figure 2b), the pseudoisoemissive point moves to 637 nm and the intensity ratio of the two bands reaches 95%. The 2.71 times increase in the fluorescence intensity of AH between excitation at 514 and 410 nm can simply be attributed to the changes in the intensity absorbed at the excitation wavelength owing to differences of molar absorption coefficients. At 410 nm, the molar absorption coefficient of AH ($\epsilon_{AH(410nm)} = 5600$ $M^{-1}$ $cm^{-1}$), determined by absorption data treatment (see above), is 22% lower than that of A ($\epsilon_{A(410nm)} = 7200$ $M^{-1}$ $cm^{-1}$), whereas, at 514 nm, $\epsilon_{AH}$ is more than two times higher than $\epsilon_A$ ($\epsilon_{AH(514nm)} = 21\,500$ $M^{-1}$ $cm^{-1}$, $\epsilon_{A(514nm)} = 10\,300$ $M^{-1}$ $cm^{-1}$). These changes lead to a 2.68 relative increase of $\epsilon_{AH}$ relative to $\epsilon_A$ upon going from 514 to 410 nm, which corresponds well with the apparent fluorescence changes observed. pH-related variations of the fluorescence intensity were analyzed taking into consideration a single equilibrium between A and AH species, using a similar treatment as that for the absorption data processing. Adjustment of the experimental data was performed simultaneously at 22 wavelengths for each of the 410 and 514 nm excitation wavelengths. Good fits were obtained as

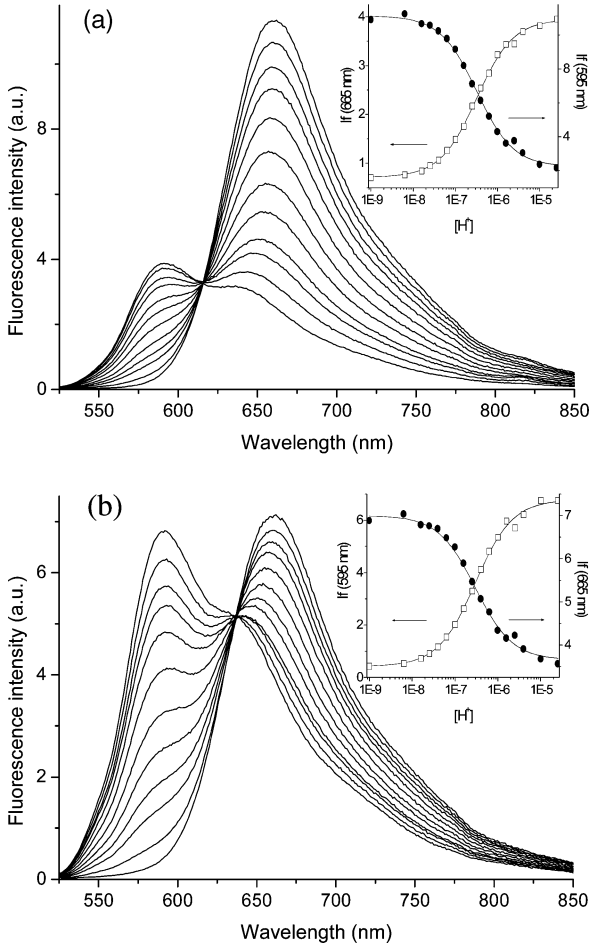


**Figure 2.** Fluorescence spectra of carboxy SNARF-4F ($1.3 \times 10^{-6}$ M) in pH buffered solutions upon excitation at 410 nm (a) and 514 nm (b). From top to bottom (at 660 nm): pH 8.2, 7.6, 7.2, 7.0, 6.8, 6.6, 6.4, 6.2, 6.0, 5.6, 5.4, and 5.0. Insets: emission of carboxy SNARF-4F versus $H^+$ concentration at 595 nm (●) and 665 nm (□). The symbols represent experimental data, and the solid lines were calculated by fitting the data.

exemplified in the insets of Figure 2. The calculated association constant was $(3.12 \pm 0.10) \times 10^6$ $M^{-1}$ ($pK_{a1} = 6.49$) and $(3.30 \pm 0.10) \times 10^6$ $M^{-1}$ ($pK_{a1} = 6.52$) for excitation at 410 and 514 nm, respectively, which agrees very well with the value derived from the pH dependence of the absorption spectra.

Protolytic equilibria in the excited state are very often different from those in the ground state owing to charge redistribution taking place after light excitation.[39] Here, the value of the association constant does not significantly differ depending on whether it was determined by absorption or by fluorescence spectroscopy. This might suggest either that protolytic equilibria in the ground and excited states are rather similar or that the equilibrium has no time to be established in the excited sate prior to deactivation of A* and AH*. The intersection point of the normalized absorption and emission spectra reconstructed from the data treatments permits the 0−0 energy transition of the A and AH forms to be estimated at 16 194 and 17 544 $cm^{-1}$, respectively. The excited-state protolytic constant ($pK_{a1}$*) predicted by means of the Förster cycle[40] would then be 3.66 ($pK_{a1} - 2.83$). This theoretical value suggests that deprotonation can occur in the excited state in the low pH range, which is apparently not the case. This supports the assumption that the equilibrium is not reached in the excited state. Evidence for the nonestablishment of the excited-state equilibrium can be found in the dependence of the emission

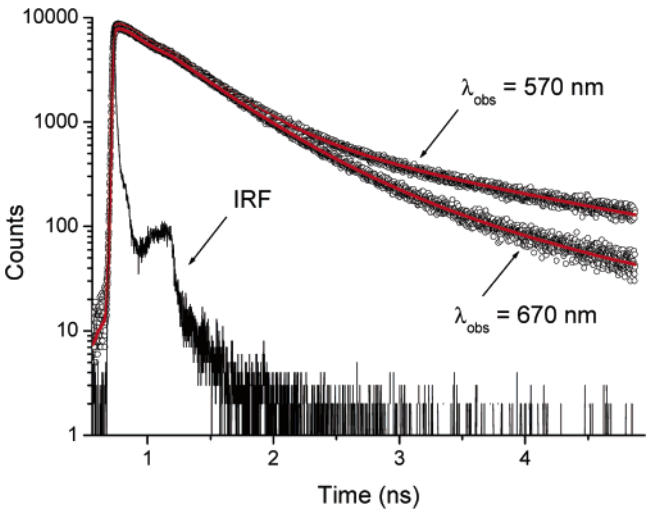


**Figure 3.** Fluorescence decays of carboxy SNARF-4F ($1.3 \times 10^{-6}$ M) at pH 5.6 observed at 570 nm (top curve) and 670 nm (bottom curve) upon excitation at 323 nm, plotted on a semilogarithmic scale. The instrumental response function (IRF) is shown. The symbols (○) represent the experimental data, and the solid lines represent the fits obtained from the multiexponential global analysis.

spectra on excitation wavelength (compare parts a and b of Figure 2) and from the fact that the fluorescence intensity as a function of pH strictly follows the concentration of the species in the ground state. Moreover, the rate for a homogeneous protonation, assuming a bimolecular diffusion-controlled rate constant of $\sim 5 \times 10^{10}$ $M^{-1}$ $s^{-1}$,[41] would be $1.2 \times 10^5$ $s^{-1}$ for a pH 5.6 solution, which is much slower than the measured fluorescence rate of both the acid and base forms ($\sim 2 \times 10^9$ $s^{-1}$, see the next section). Deprotonation in the excited state, which would be expected at pH values down to ~3.6, is apparently too slow to have a noticeable influence on the spectra.

**Time-Resolved Fluorescence Spectroscopy.** Fluorescence decay traces of carboxy SNARF-4F ($1.3 \times 10^{-6}$ M) in solution buffered at different pHs were recorded at 570, 625, and 670 nm upon excitation at 323 nm using the TCSPC setup (see the Experimental Section) and by using the confocal microscope setup depicted in Scheme 2 ($\lambda_{ex} = 514$ nm). The latter permits the fluorescence of the short- and long-wavelength bands to be separated, at least partly, on two detectors. At both pumping wavelengths, the AH form is preferentially excited (see Figure 1), whereas emission observed in the short- and long-wavelength bands, respectively, optimizes the detection of the protonated and unprotonated species.

Upon excitation at 323 nm, the decay of the pH 8.2 solution was found to be monoexponential at 670 nm with a fluorescence lifetime ($\tau$) of 0.68 ns. At this pH, the concentration of A in the ground state represents 98% of the total fluorophore concentration. At 570 nm, the emission intensity was too low to be monitored. At pH 5.6 (90.6% of AH in the ground state), the fluorescence decays observed at 570 and 670 nm exhibited a nonexponential behavior (Figure 3), which could only be fitted by taking into account a biexponential model with decay times of 0.41 and 1.87 ns at 570 nm and 0.44 and 1.23 ns at 670 nm. For intermediate pHs, decays observed at 570 nm all exhibited lifetimes and preexponential factors similar to the pH 5.6 solution, within experimental error. The experimental fluorescence decays recorded at various pHs upon excitation at 323 nm and observed at the three wavelengths were analyzed globally with the lifetimes linked to determine the values more accurately. The normalized preexponential factors and the decay times obtained from the fitting procedure are gathered in Table 1. The three decay times are close to the values discussed above: $\tau_1 = 0.40$ ns and $\tau_2 = 1.87$ ns correspond well to the decay obtained at pH 5.6 ($\lambda_{em} = 570$ nm), and $\tau_3 = 0.73$ ns corresponds well to the decay at pH 8.2 ($\lambda_{em} = 670$ nm). At 625 and 670 nm, the $\tau_1$ amplitude drops with increasing pH, whereas the $\tau_3$ amplitude increases. These amplitude changes are particularly attractive, since they allow one to construct a pH calibration curve, making carboxy SNARF-4F a suitable probe for lifetime-based sensing.

**TABLE 1: Results of the Multiexponential Global Analysis of the Experimental Picosecond Decay Traces Recorded at Various pHs and Observation Wavelengths upon Excitation at 323 nm[a]**

| | $\lambda_{em} = 570$ nm | | | $\lambda_{em} = 625$ nm | | | $\lambda_{em} = 670$ nm | | |
|---|---|---|---|---|---|---|---|---|---|
| pH | $\alpha_1$ | $\alpha_2$ | $\alpha_3$ | $\alpha_1$ | $\alpha_2$ | $\alpha_3$ | $\alpha_1$ | $\alpha_2$ | $\alpha_3$ |
| 5.6 | 0.911 | 0.089 | | 0.864 | 0.027 | 0.019 | 0.779 | 0.019 | 0.202 |
| 6.0 | 0.902 | 0.098 | | 0.826 | 0.027 | 0.147 | 0.669 | 0.016 | 0.315 |
| 6.4 | 0.906 | 0.094 | | 0.719 | 0.028 | 0.253 | 0.510 | 0.010 | 0.480 |
| 6.8 | 0.904 | 0.096 | | 0.592 | 0.022 | 0.386 | 0.362 | | 0.638 |
| 7.0 | 0.893 | 0.107 | | 0.436 | 0.018 | 0.546 | 0.254 | | 0.746 |
| 7.4 | | | | 0.326 | | 0.674 | 0.184 | | 0.816 |
| 8.2 | | | | 0.207 | | 0.793 | 0.150 | | 0.850 |

[a] $\alpha_1$, $\alpha_2$, and $\alpha_3$ are the normalized preexponential factors ($\alpha_i/\Sigma\alpha_i$) referring to $\tau_1 = 0.40$ ns, $\tau_2 = 1.87$ ns, and $\tau_3 = 0.73$ ns, respectively. The global residual was $\chi_r^2 = 1.14$.

From our measurements, we did not observe negative preexponential factors, which usually characterize excited-state proton transfer reactions. In the absence of such a reaction, A* and AH* are not coupled and decay independently of each other. Good fits were attained here with pH-independent decay times, so that the recovered decay times should correspond to those of the unprotonated and protonated forms. The 0.73 ns lifetime ($\tau_3$), only observed at 625 and 670 nm, can be ascribed to the excited state of A. Additional evidence for the assignment of $\tau_3$ to A* can be found from the pH dependence of the preexponential factor $\alpha_3$, the amplitude of which decreases with pH (Table 1), that is, with the concentration of A in the ground state. At 570 nm, where A* can be considered as nonemitting, a biexponential decay with the decay times $\tau_1$ and $\tau_2$ is obtained. Whitaker et al.[9] also observed for several benzo[*c*]xanthene dyes a biexponential decay of the fluorescence, reminiscent to what we observed here for the protonated carboxy SNARF-4F. They assigned it to fluorescent impurity traces and scattering of light. In the present work, the purification achieved on the compound before use and the large contribution to the fluorescence (~30%) found for the $\tau_2$ component allow us to reasonably discard any residual impurities to account for the biexponential law obtained.

The preexponential factors of $\tau_1$ and $\tau_2$, 90.3 and 9.7% on average at 570 nm, respectively, do not evolve with pH. This pH independence also strongly supports the absence of fluorescent impurities. At 625 and 670 nm, the amplitude of $\tau_2$ is 3.5% (625 nm) and 2.2% (670 nm) on average of that of $\tau_1$, respectively, below pH 7 and pH 6.4. At higher pH values, it was not necessary to include the contribution of $\tau_2$ to improve the quality of the fits. This component would have contributed to less than 1% of the total amplitude, assuming the ratio of the amplitudes of $\tau_1$ and $\tau_2$ is the same as that at lower pH. In any case, the pH independence of the $\tau_1$ and $\tau_2$ amplitudes observed at each wavelength indicates that these decay times are associated with each other. Such a behavior is expected if an equilibrium between two species is involved, either in the ground or in the excited state. Note that in the case of an excited-state equilibrium the species do not necessarily need to be both fluorescing for a biexponential decay law to be observed. In

**TABLE 2: Results of the Fits of the Experimental Sub-nanosecond Decay Traces Recorded at Various pHs and Observed Simultaneously on SPAD 1 (D660/50m filter) and SPAD 2 (D580/25m filter) upon Excitation at 514 nm[a]**

| | SPAD 1 | | | SPAD 2 | | |
|---|---|---|---|---|---|---|
| pH | $\alpha_1$ | $\alpha_2$ | $\alpha_3$ | $\alpha_1$ | $\alpha_2$ | $\alpha_3$ |
| 5.6 | 0.822 | 0.026 | 0.152 | 0.953 | 0.047 | |
| 6.2 | 0.686 | 0.019 | 0.295 | 0.949 | 0.051 | |
| 6.4 | 0.619 | 0.017 | 0.364 | 0.926 | 0.051 | 0.023 |
| 6.6 | 0.544 | 0.015 | 0.441 | 0.924 | 0.052 | 0.024 |
| 6.8 | 0.445 | 0.012 | 0.543 | 0.905 | 0.054 | 0.041 |
| 7.0 | 0.435 | 0.011 | 0.554 | 0.870 | 0.060 | 0.070 |
| 7.4 | 0.309 | 0.006 | 0.685 | 0.811 | 0.064 | 0.125 |
| 8.2 | 0.261 | 0.003 | 0.736 | 0.486 | 0.061 | 0.453 |

[a] $\alpha_1$, $\alpha_2$, and $\alpha_3$ are the normalized preexponential factors ($\alpha_i/\Sigma\alpha_i$) referring to $\tau_1 = 0.40$ ns, $\tau_2 = 1.98$ ns, and $\tau_3 = 0.75$ ns, respectively.

the next paragraphs, we consider the existence of ground- and excited-state equilibria as a potential explanation for the biexponential decay having pH-independent amplitudes. The existence of isomers is also envisaged, and factors that might influence the decays, like the presence of proteins, are discussed.

If an equilibrium in the ground state only is concerned, it has to be pH-independent and the involved species must exhibit a fluorescence in the same spectral range as AH*. As a pH-independent process, one may think of an equilibrium between AH and/or A species and the previously mentioned colorless lactone form. Lactones, either in rhodamines or triarylmethane dyes,[42,43] are indeed characterized by a pronounced Stokes shift, which reaches, for example, $\sim$12 000 cm$^{-1}$ for the lactone rhodamine 101 in methyltetrahydrofuran.[44] Under these circumstances, excitation in the visible part of the absorption spectrum, where the lactone form does not absorb, must result in the observation of a single monoexponential decay of the blue-shifted emission band. The existence of the ground-state lactone was investigated by recording fluorescence decay traces in the short- and long-wavelength bands upon excitation at 514 nm. From a multiexponential global fit (Table 2), decay times ($\tau_1 = 0.40$, $\tau_2 = 1.98$, and $\tau_3 = 0.75$ ns) similar to those obtained upon 323 nm excitation were determined. The slightly larger $\tau_2$ value might just reflect a better accuracy of the measured decay in the longer experimental time window used ($\sim$13 ns for the 514 nm excitation vs $\sim$5 ns at 323 nm). Moreover, the small decreases in the $\tau_1$ amplitude relative to $\tau_2$ on SPAD 2, especially for the highest pHs, are merely due to a large error on the amplitude determination and are consequently not considered to be significant. The two decay times measured in the short-wavelength fluorescence band exclude the biexponential decay observed upon excitation at 323 nm ($\lambda_{obs} = 570$ nm) to come from a ground-state equilibrium involving the lactone form. This is also supported by their amplitudes ($\alpha_1 = 95.3\%$ and $\alpha_2 = 4.7\%$ at pH 5.6) which are close to those obtained after 323 nm excitation.

In the case the equilibrium involves an excited-state reaction of second or pseudo-first order, factors such as dye or buffer concentration should influence the deactivation kinetics of the excited states. For instance, catalysis of the excited-state proton transfer reaction of the carboxy SNAFL-1 parent compound by buffer ions is expected at buffer concentrations over 50 mM.[9] The fluorescence decay of a nonbuffered aqueous solution (pH 7) of carboxy SNARF-4F ($1.3 \times 10^{-6}$ M) recorded upon excitation at 514 nm and detected on SPAD 2 could be fitted with three decay times: $\tau_1 = 0.38$ ns, $\tau_2 = 2.03$ ns, and $\tau_3 = 0.78$ ns. The decays of a much lower dye concentration ($8.75 \times 10^{-9}$ M) buffered at pH 5.6, 6.0, 6.6, 7.4, and 8.2 (10 mM) could be fitted simultaneously on both SPADs with decay times ($\tau_1 = 0.39$ ns, $\tau_2 = 1.91$ ns, and $\tau_3 = 0.79$ ns) similar to those of the unbuffered solution. These results, which are very close to those obtained before for a micromolar concentration of the dye ($\tau_1 = 0.40$ ns, $\tau_2 = 1.98$ ns, and $\tau_3 = 0.75$ ns), argue in favor of an excited-state equilibrium that does not involve buffer ions and emphasize the monomolecular character of the forward and backward reactions.

It is worth noting that carboxy SNARF-4F is a mixture of two isomers. These isomers, which are borne by the phthalide part of the molecule perpendicular to the planar xanthene skeleton, are expected to possess similar spectroscopic and photophysical properties. For instance, the 5- and 6-isomers of carboxyfluorescein exhibit the same lifetime of 4 ns.[45,46] It is thus unlikely that the $\tau_1$ and $\tau_2$ lifetimes can result from structural differences between the two isomers. The biexponential behavior observed in the emission spectral range of AH* might then better be attributed to dynamic processes taking place in the excited state.

Many rhodamine-like fluorophores have been reported to exhibit an additional distinct fluorescence lifetime upon binding to proteins such as bovine serum albumin (BSA). For instance, in addition to the lifetimes of the protonated (0.5−0.6 ns) and unprotonated ($\sim$1.5 ns) forms of carboxy SNARF-1, a third longer decay time of 3−4 ns was reported and attributed to bound populations of the dye.[47,48] In solution free from protein, our study on carboxy SNARF-4F reveals at most three decaying components. To verify the influence of proteins on the decays, we recorded fluorescence decay times in the presence of BSA at a pH (5.6) and for a wavelength (detection on SPAD 2) at which the bound population is expected to emit.[48] Decays of a $8.75 \times 10^{-9}$ M solution ($\lambda_{exc} = 514$ nm) in the presence of BSA up to $5 \times 10^{-6}$ M showed a biexponential behavior, the lifetimes (0.43 and 2.10 ns) and amplitudes (93 and 7%, respectively) of which were very close to those measured in the absence of BSA (Table 2). This suggests no noticeable interaction of the protein with the probe. The three lifetimes we measured in the presence of BSA are thus intrinsic to the fluorophore, in contrast to what is reported for other dyes of the same family.

**Modeling and Fitting the Time-Resolved Fluorescence Data.** A global modeling (see the Experimental Section for details of the procedure) of the experimental picosecond fluorescence decays recorded after excitation at 323 nm was performed. The kinetic model (Scheme 3) involves pumping of the A and AH forms according to their pH-dependent ground-state concentrations, the subsequent decays to the ground state, and one more step describing an equilibrium between AH* and a species denoted as Y* also able to return to the ground state. Scheme 3 should be considered as the simplest model able to satisfactorily account for the dynamical behavior of carboxy SNARF-4F in low-buffered solutions. Fitting of the kinetic data was simultaneously performed at the three wavelengths for the seven different pH values reported in Table 1. Attempts to adjust the 570 nm data to the full kinetic model were unsuccessful owing to the presence of the $k_4$ deactivation constant. The decay rate of Y*, probably too slow to be reliably measured in the time window of the experiment, was then arbitrarily fixed at $1 \times 10^{-59}$ s$^{-1}$.

In a first step, data at the three emission wavelengths were fitted independently. In this case, the parameter corresponding to the fluorescence emission coefficient of Y* ($q_{Y^*}$) was not necessary to correctly reproduce the data. The fluorescence

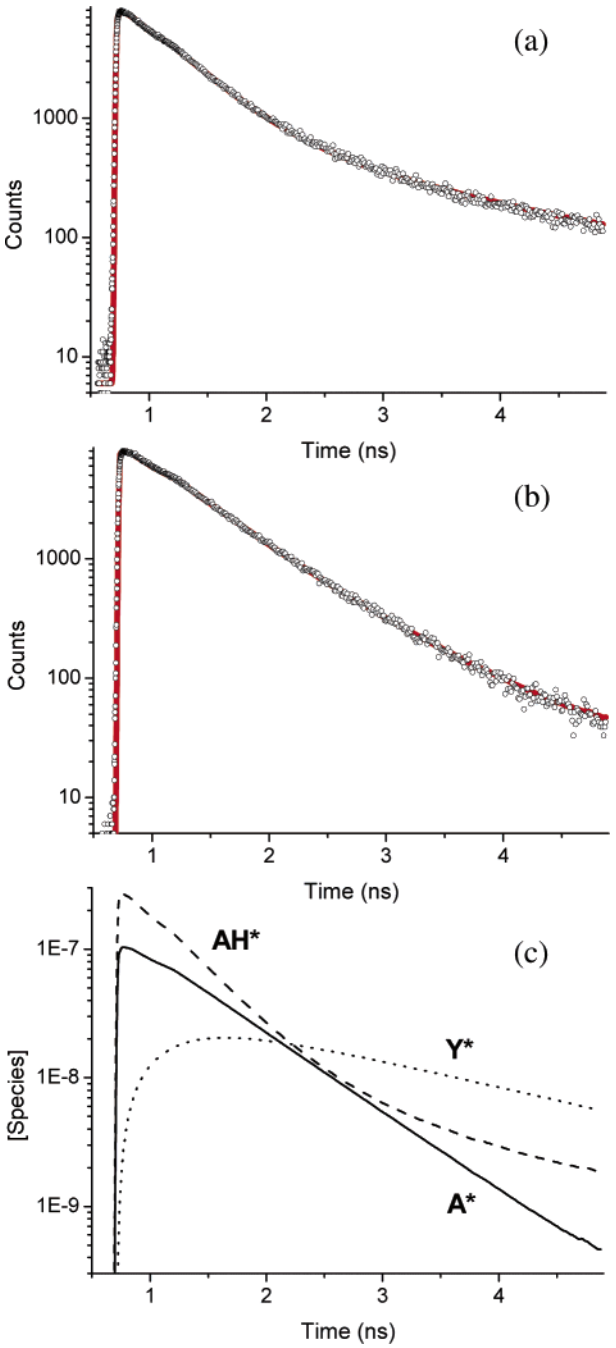


**Figure 4.** Fluorescence decays of carboxy SNARF-4F ($1.3 \times 10^{-6}$ M) at pH 6.4 observed at 570 nm (a) and 670 nm (b) upon excitation at 323 nm. The symbols (○) represent the experimental data, and the solid lines represent the fits obtained from the kinetic modeling. (c) Calculated concentration profiles of the species in the excited state convoluted by the instrumental response function.

decays observed at 570 nm could be fitted by taking into account emission from AH* species only. This means that the observed biexponential behavior simply return the excited-state concentration profile of the AH species. Emission from both the A* and AH* forms was necessary at 625 and 670 nm. In a second step, attempts to *simultaneously* fit the three wavelengths by omitting the spontaneous emission coefficient of Y* ($q_{Y^*}$) resulted in poor fits. In the last step, $q_{Y^*}$ was taken into consideration. Excellent fits were obtained at all the wavelengths, as exemplified in Figure 4 for the pH 6 solution. The need of Y* fluorescence in the fitting process can be understood by comparing the 570 and 670 nm decay profiles of the pH 5.6 solution shown in Figure 3. At pH 5.6, the solution contains 90.6% of AH in the ground state. If we assume that the kinetic trace observed at 570 nm only returns the concentration profile of AH* ($0.911 \exp(-t/\tau_1) + 0.089 \exp(-t/\tau_2)$, see Table 1), the same AH* profile is expected at 670 nm in addition to that of A*. The drop in the relative proportion of the $\tau_2$ amplitude respective to $\tau_1$, from 8.9 to 2.4% going from 570 to 670 nm, indicates that a species different from AH* has to fluoresce for a good fit to be obtained simultaneously at both wavelengths.

**TABLE 3: Optimized Time Constants ($k_i$) and Spontaneous Emission Coefficients ($q_i$) Calculated from the Simultaneous Fit of the Data of Table 1 (pH and Observation Wavelengths) According to Scheme 3 ($\lambda_{ex} = 323$ nm)**

| | $q_i$ ($10^{10}$) | | |
|---|---|---|---|
| | 570 nm | 625 nm | 670 nm |
| $q_{A^*}$ | 0 | 1.64 | 3.89 |
| $q_{AH^*}$ | 3.04 | 2.29 | 1.28 |
| $q_{Y^*}$ | 1.52 | 0.11 | 0.0001 |

| | $k_i$ ($10^9$ s$^{-1}$) |
|---|---|
| $k_2$ | $0.19 \pm 0.03$ |
| $k_{-2}$ | $0.53 \pm 0.03$ |
| $k_3$ | $2.13 \pm 0.07$ |
| $k_5$ | $1.47 \pm 0.05$ |

The optimized rate constants and fluorescence emission coefficients calculated from the treatment are given in Table 3. The fluorescence decay times of the protonated species calculated from the optimized rate constants ($\tau = (k_2 + k_3)^{-1} = 0.43$ ns and $\tau = (k_{-2})^{-1} = 1.88$ ns) are in good agreement with the values obtained by the multiexponential global analysis ($\tau_1 = 0.40$ and $\tau_2 = 1.87$ ns) as well as the fluorescence decay time of A* ($\tau = (k_5)^{-1} = 0.68$ ns vs $\tau_3 = 0.73$ ns). The emission coefficient ratio Y*/AH* decreases going from 570 to 670 nm, which supports the $\tau_2$ amplitude decrease obtained by the previous analysis. Figure 4 depicts the concentration profile of the A*, AH*, and Y* species obtained by the calculation, from which the building-up of the Y* species can clearly be seen. To define how critical the $k_4$ constant setting is on the fits, we performed some fits by changing its value, keeping the other deactivation constants at their adjusted values. It appeared that increasing $k_4$ up to $5 \times 10^7$ s$^{-1}$ did not result in any noticeable changes in the quality of the fits.

As an assignment for the Y* state, one might consider the formation, in the excited state, of the lactone form in equilibrium with the excited protonated carboxy SNARF-4F. Compared to the numerous investigations carried out on the photophysical properties of the zwitterionic form of rhodamine derivatives, the lactone form has been the subject of only a few studies.[38,44,49,50] For rhodamine 101, the parent compound of rhodamine B with amino groups rigidly linked to the xanthene skeleton, it has been shown that excitation of the lactone is followed by an electron transfer from the xanthene to the phthalide moiety, from which the highly polar excited charge transfer state and the zwitterion excited state can be populated.[44] The reversibility of the two emitting states has been strongly suggested in refs 44 and 49 to explain some spectroscopic data, but direct experimental proof of the mutual coupling was never reported. The biexponential decay behavior observed in the emission spectral range of AH* could simply reflect an equilibrium in the excited state between AH* and the lactone, as supported by our time-resolved data modeling. Closing of the lactone ring might be produced only from the protonated carboxy SNARF-4F, and not from the unprotonated dye, because of a cyclization facilitated by the presence of a partial positive charge at the carbon atom in the 9 position of the xanthene

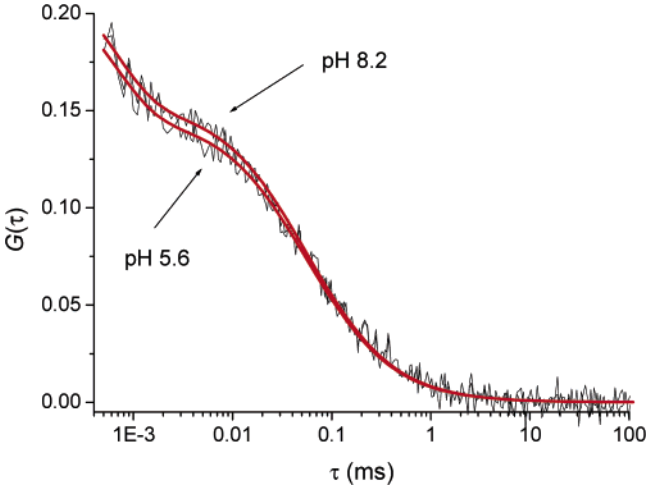


**Figure 5.** Fluorescence autocorrelation curves of carboxy SNARF-4F at pH 5.6 and 8.2 recorded on SPAD 1. The solid lines are the fits obtained according to eq 2.

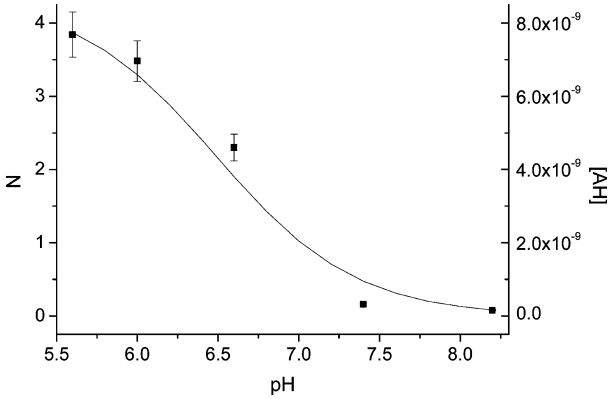


**Figure 6.** Mean number of molecules (*N*) detected on SPAD 2 and theoretical concentration of the acid form of carboxy SNARF-4F versus pH.

part (Scheme 1). The value of the excited-state equilibrium constant defined by $k_{-2}/k_2$ would be 2.5, which could very well correspond to a lactone-to-acid equilibrium, AH* ⇄ Y*. As a matter of fact, that of the ground state of the parent compound rhodamine B is reported to be 4.4 in water.[38] The slow deactivation rate constant of the lactone excited state ($\tau_f$ > 20 ns) would also agree with the reported (3−6) × $10^6$ $s^{-1}$ radiative rate constant of rhodamine derivatives.[51]

An alternative assignment of Y* could be seen in the basic Eigen[52] and Weller[53] picture of an excited-state proton transfer (ESPT) reaction, which involves a two-step reaction scheme: a fast dissociation of the acid producing a contact ion pair, $A^-\cdot\cdot\cdot H^+$, and the subsequent geminate recombination process is followed by a reversible diffusive stage. The ESPT first requires the primary formation of a H-bonded complex, AH···S, between the acid form and, for instance, a proton acceptor solvent, S. Global modeling of the time-resolved fluorescence data revealed that Y* emits in the same spectral range as the AH species. This confirms that the intrinsic proton transfer step has not occurred, since it would have produced a contact ion pair, $A^-{}^*\cdot\cdot\cdot HS^+$, whose spectral properties would resemble more those of $A^-$. A possible attribution for the Y* species would then be the H-bonded complex, AH···S, which would possess photophysical properties more similar to those of AH* than of A* or its H-bonded complex, $A^-{}^*\cdot\cdot\cdot HS^+$. In that case, however, the long excited-state lifetime is unexpected. Recently, Rini et al.[54] reported the slow formation of a collision complex involving extensive solvent reorganization on a time scale slower than the few hundred femtoseconds it requires for the proton transfer step. Owing to the lack of buffer influence on the deactivation of the excited states, the formation of such a complex seems unlikely. Moreover, the time-resolved kinetics of the acid and base excited states of an ESPT are expected to exhibit an asymptotic long time behavior respectively obeying a $t^{-3/2}$ and a $t^{-1/2}$ power law,[55] which are absent from our measurements.

**Fluorescence Correlation Spectroscopy.** The 514 nm excitation wavelength permits traces of the acid form of carboxy SNARF-4F to be efficiently detected (Figure 2b). Fluctuations of the dye fluorescence (8.75 × $10^{-9}$ M) were monitored on SPAD 1 and 2 (Scheme 2) for different buffer concentrations. The autocorrelation functions recorded on SPAD 1 are independent of the pH of the solution. As an example, Figure 5 depicts the FCS curves obtained at pH 5.6 and 8.2 (unnormalized amplitudes), from which a fluorescence flickering process (microsecond time range) in addition to the translational diffusion in and out the sample volume element (∼50 $\mu$s) can be observed. The FCS curves recorded for five different pHs ranging from 5.6 to 8.2 were analyzed simultaneously using eq 2. The diffusion coefficient was found to be (2.10 ± 0.05) × $10^{-6}$ $cm^2/s$, which is close to that of R6G in water (2.8 × $10^{-6}$ $cm^2/s$),[28] and the estimated flicker time was $\tau \sim 0.70 \pm 0.05$ $\mu$s with a dark molecular fraction of ∼35%. Note that the last time constant is of the order of magnitude of the characteristic triplet−singlet transitions of a large number of fluorescent dyes. The formation of the triplet state was checked by increasing the illumination intensity (below the optical saturation) which resulted in a slight increase of the dark-state population. This is consistent with triplet formation, even if a full characterization of the process merits further investigation. The dynamic processes of the FCS curves obtained on SPAD 2 resembled those of Figure 5 and could be fitted with the same time constants. Only the amplitudes varied, decreasing from 3.84 at pH 5.6 to 0.08 for a pH 8.2 solution. The amplitude changes reflect the actual increase of the mean number of molecules (*N*) of the acid form within the sample volume expected upon a decrease of the pH of the solution. Figure 6 shows the values of *N* obtained between pH 5.6 and pH 8.2 together with the pH-dependent acid form concentration. Good agreement is obtained between the measured and the calculated values.

In contrast to the kinetics observed in protein pH sensors such as GFPs, the fluorescence fluctuations observed here are independent of the pH of the solution.[56] Therefore, the relaxation rate of the protolytic equilibrium cannot be determined. For proteins, the protonation and deprotonation rate constants are on the order of $10^9$ $M^{-1}$ $s^{-1}$ and (1−100) × $10^2$ $s^{-1}$, respectively.[23,56,57] A possible explanation for the absence of the protonation/deprotonation kinetics on the FCS curves of carboxy SNARF-4F might be the values of the rate constants, too high to be observed with our setup. The slowest process determined by the time-resolved experiments, $k_2$ of the kinetic model of Scheme 3, is ∼2 × $10^8$ $s^{-1}$, which is still too fast to be detectable in our FCS experiments. Moreover, it should be mentioned that obtaining correlation curves with a good signal-to-noise ratio required a long acquisition time. This could be due to the rather low molecular brightness of the dye and would therefore limit the use of SNARF-4F as a freely diffusing pH probe in single-molecule experiments.

## Conclusion

The steady-state spectroscopic properties of 2-[10-(dimethylamino)-4-fluoro-3-oxo-3H-benzo[*c*]xanthen-7-yl] (carboxy SNARF-4F) in aqueous buffered solutions are greatly affected by the presence of the hydronium ion. Protonation of the compound results in a blue shift of both the UV−vis absorption and fluorescence spectra. From time-resolved fluorescence measurements on the picosecond time scale, it was shown that protonated and unprotonated forms of carboxy SNARF-4F exhibit different decay times. In addition, the fluorescence decays of AH* revealed the presence of a long lifetime component ($\tau_2 = 1.85$ ns), whose amplitude is independent of the pH of the solution ($\alpha_2 \sim 10\%$ at 570 nm). A global analysis procedure of the time-resolved data was undertaken to account for the observed behavior. The selected kinetic model, which permits one to satisfactorily fit the data, takes into account an equilibrium between the excited protonated form of carboxy SNARF-4F and a species denoted as Y*, which is produced in the excited state. The Y* species was tentatively ascribed to the lactone form or to a complex formed by hydrogen bonding with the surrounding solvent molecules. The peculiar steady-state and time-resolved behavior makes carboxy SNARF-4F a unique fluorescent sensor for measuring pH by combining the advantages of wavelength ratiometric and fluorescence decay time measurements.

**Acknowledgment.** We thank Dick Bebelaar and John van Ramesdonk for help with the experimental setup. N.M. is grateful to Dominique Lavabre for encouragements and for kindly assisting her during modeling and fitting of the data. This research was financially supported by the Netherlands Research School Combination Catalysis (NRSCC).

## References and Notes

(1) Wolfbeis, O. S. *Springer Ser. Chem. Sens. Biosens.* **2004**, *1*, 1.
(2) Epstein, J. R.; Walt, D. R. *Chem. Soc. Rev.* **2003**, *32*, 203.
(3) Lin, J. *Trends Anal. Chem.* **2000**, *19*, 541.
(4) Thompson, R. B.; Lakowicz, J. R. *Anal. Chem.* **1993**, *65*, 853.
(5) Moerner, W. E.; Fromm, D. P. *Rev. Sci. Instrum.* **2003**, *74*, 3597.
(6) Ambrose, W. P.; Goodwin, P. M.; Jett, J. H.; Van Orden, A.; Werner, J. H.; Keller, R. A. *Chem. Rev.* **1999**, *99*, 2929.
(7) Boehmer, M.; Enderlein, J. *ChemPhysChem* **2003**, *4*, 792.
(8) Weiss, S. *Science* **1999**, *283*, 1676.
(9) Whitaker, J. E.; Haugland, R. P.; Prendergast, F. G. *Anal. Biochem.* **1991**, *194*, 330.
(10) Cody, S. H.; Dubbin, P. N.; Beischer, A. D.; Duncan, N. D.; Hill, J. S.; Kaye, A. H.; Williams, D. A. *Micron* **1993**, *24*, 573.
(11) Roberts, E. L., Jr. *Methods* **1999**, *18*, 150.
(12) Albrechtova, J. T. P.; Heilscher, S.; Leske, L.; Walczysko, P.; Wagner, E. *Plant, Cell Environ.* **2003**, *26*, 1985.
(13) Chen, F. F. T.; Dilworth, E.; Swietach, P.; Goddard, R. S.; Vaughan-Jones, R. D. *J. Physiol. (Cambridge, U. K.)* **2003**, *552*, 715.
(14) Vaughan-Jones, R. D.; Peercy, B. E.; Keener, J. P.; Spitzer, K. W. *J. Physiol. (Cambridge, U. K.)* **2002**, *541*, 139.
(15) Gulcev, M.; Goring, G. L. G.; Rakic, M.; Brennan, J. D. *Anal. Chim. Acta* **2002**, *457*, 47.
(16) Liu, J.; Diwu, Z.; Leung, W.-Y. *Bioorg. Med. Chem. Lett.* **2001**, *11*, 2903.
(17) Lippitsch, M. E.; Draxler, S.; Kieslinger, D. *Sens. Actuators, B* **1997**, *38*, 96.
(18) de Silva, A. P.; Gunaratne, H. Q. N.; Gunnlaugsson, T.; Lynch, P. L. M. *New J. Chem.* **1996**, *20*, 871.
(19) Fabbrizzi, L.; Gatti, F.; Pallavicini, P.; Parodi, L. *New J. Chem.* **1998**, *22*, 1403.
(20) Gao, X.; Zhang, Y.; Wang, B. *Org. Lett.* **2003**, *5*, 4615.
(21) Szmacinski, H.; Lakowicz, J. R. *Anal. Chem.* **1993**, *65*, 1668.
(22) Draxler, S.; Lippitsch, M. E.; Leiner, M. J.-P. *Sens. Actuators, B* **1993**, *11*, 421.
(23) Hess, S. T.; Heikal, A. A.; Webb, W. W. *J. Phys. Chem. B* **2004**, *108*, 10138.
(24) McAnaney, T. B.; Park, E. S.; Hanson, G. T.; Remington, S. J.; Boxer, S. G. *Biochemistry* **2002**, *41*, 15489.
(25) Hanson, G. T.; McAnaney, T. B.; Park, E. S.; Rendell, M. E. P.; Yarbrough, D. K.; Chu, S.; Xi, L.; Boxer, S. G.; Montrose, M. H.; Remington, S. J. *Biochemistry* **2002**, *41*, 15477.
(26) van Dijk, S. I.; Wiering, P. G.; Groen, C. P.; Brouwer, A. M.; Verhoeven, J. W.; Schuddeboom, W.; Warman, J. M. *J. Chem. Soc., Faraday Trans.* **1995**, *91*, 2107.
(27) Hess, S. T.; Webb, W. W. *Biophys. J.* **2002**, *83*, 2300.
(28) Rigler, R.; Mets, U.; Widengren, J.; Kask, P. *Eur. Biophys. J.* **1993**, *22*, 169.
(29) Janssens, L. D.; Boens, N.; Ameloot, M.; De Schryver, F. C. *J. Phys. Chem.* **1990**, *94*, 3564.
(30) Zuker, M.; Szabo, A. G.; Bramall, L.; Krajcarski, D. T.; Selinger, B. *Rev. Sci. Instrum.* **1985**, *56*, 14.
(31) Kaps, K.; Rentrop, P. *Comput. Chem. Eng.* **1984**, *8*, 393.
(32) Ramette, R. W.; Sandell, E. B. *J. Am. Chem. Soc.* **1956**, *78*, 4872.
(33) Zanker, V.; Peter, W. *Chem. Ber.* **1958**, *91*, 572.
(34) Lopez-Arbeloa, I.; Rohatgi-Mukherjee, K. K. *Chem. Phys. Lett.* **1986**, *128*, 474.
(35) Yguerabide, J.; Talavera, E.; Alvarez, J. M.; Quintero, B. *Photochem. Photobiol.* **1994**, *60*, 435.
(36) Alvarez-Pez, J. M.; Ballesteros, L.; Talavera, E.; Yguerabide, J. *J. Phys. Chem. A* **2001**, *105*, 6320.
(37) Drexhage, K. H. In *Topics in Applied Physics*; Schäffer, F. P., Ed.; Springer-Verlag: Berlin, 1977; p 143.
(38) Hinckley, D. A.; Seybold, P. G. *Spectrochim. Acta, Part A* **1988**, *44*, 1053.
(39) Parker, C. A. *Photoluminescence of Solutions*; Elsevier: Amsterdam, The Netherlands, 1968.
(40) Vander Donckt, E. *Prog. React. Kinet.* **1970**, *5*, 274.
(41) Valeur, B.; *Molecular Fluorescence. Principles and Applications*; Wiley-VCH: Weinhein, Germany, 2002.
(42) Kaneo, Y.; Neckers, D. C. *J. Phys. Chem. A* **1998**, *102*, 5356.
(43) Karpiuk, J. *Phys. Chem. Chem. Phys.* **2003**, *5*, 1078.
(44) Karpiuk, J.; Grabowski, Z. R.; De Schryver, F. C. *J. Phys. Chem.* **1994**, *98*, 3247.
(45) Vallotton, P.; Vogel, H. *J. Fluoresc.* **2000**, *10*, 325.
(46) Lakowicz, J. R.; Castellano, F. N.; Dattelbaum, J. D.; Tolosa, L.; Rao, G.; Gryczynski, I. *Anal. Chem.* **1998**, *70*, 5115.
(47) Srivastava, A.; Krishnamoorthy, G. *Anal. Biochem.* **1997**, *249*, 140.
(48) Praus, P.; Sureau, F. *J. Fluoresc.* **2000**, *10*, 361.
(49) Karpiuk, J.; Grabowski, Z. R.; De Schryver, F. C. *Proc. Indian Acad. Sci.* **1992**, *104*, 133.
(50) Klein, U. K. A.; Hafner, F. W. *Chem. Phys. Lett.* **1976**, *43*, 141.
(51) Grabowski, Z. R.; Rotkiewicz, K.; Rettig, W. *Chem. Rev.* **2003**, *103*, 3899.
(52) Eigen, M. *Angew. Chem., Int. Ed. Engl.* **1964**, *3*, 1.
(53) Weller, A. *Prog. React. Kinet.* **1961**, *1*, 187.
(54) Rini, M.; Magnes, B.-Z.; Pines, E.; Nibbering, E. T. J. *Science* **2003**, *301*, 349.
(55) Gopich, I. V.; Solntsev, K. M.; Agmon, N. *J. Chem. Phys.* **1999**, *110*, 2164.
(56) Haupts, U.; Maiti, S.; Schwille, P.; Webb, W. W. *Proc. Natl. Acad. Sci. U.S.A.* **1998**, *95*, 13573.
(57) Schwille, P.; Kummer, S.; Heikal, A. A.; Moerner, W. E.; Webb, W. W. *Proc. Natl. Acad. Sci. U.S.A.* **2000**, *97*, 151.